Hollow cathode thermal modelling and self-consistent plasma solution: two step neutralization modelling.

IEPC-2019-A-301

Presented at the 36th International Electric Propulsion Conference
University of Vienna, Austria
September 15-20, 2019

Pablo Guerrero*
California Institute of Technology, Pasadena, CA, 91001, USA.

Ioannis G. Mikellides †and James E. Polk ‡
Jet Propulsion Laboratory, Pasadena, CA, 91109, USA.

Rosa Carmina Monreal§
Universidad Autónoma de Madrid, Cantoblanco, Madrid, E28049, Spain.

and

Daniel I. Meiron¶
California Institute of Technology, Pasadena, CA, 91125, USA.

Self-heating hollow cathodes are central components in modern electric thrusters. The plasma discharge inside these devices heats the internal components, thus maintaining the temperatures required for electron emission. Precise knowledge of the physical phenomena governing hollow cathode operation, specifically, their thermionic emission characteristics, is key to predict their lifetime. A new simulation platform has been built to couple plasma and thermal physics models of the self-heating hollow cathode to produce a self-consistent solution. The plasma solution is provided by JPL's 2D axisymmetric code OrCa2D and the cathode thermal solver is facilitated by COMSOL's Multiphysics® heat transfer module. The platform allows investigation of the sensitivity of different variables that govern the behaviour of the three dominant processes involved in cathode operation - thermal, plasma and chemical.

Previous attempts to find agreement between simulation results and experimental measurements suggested that the work function might be spatially dependent and/or the heat fluxes from the plasma to the internal walls of the cathode were overestimated.

In this work we explore the dependence of the spatial variations of the work function along the thermionic emitting surface and the effect of the ion accommodation factor when resonant neutralization is assumed. Additionally, we explore the effect of a two step neutralization process of the returning ion fluxes that dominates the heat loads to the cathode structure. The two step neutralization process, including resonant neutralization to the first excited state of xenon, followed by Auger de-excitation to the ground state, was modelled and simulated in the new computational platform. The result matches the

*Postdoctoral researcher, Aerospace, Caltech, pguerrer@caltech.edu
†Principal Engineer, Propulsion and Materials Engineering Section, JPL, ioannis.g.mikellides@jpl.nasa.gov
‡Principal Engineer, Propulsion and Materials Engineering Section, JPL, james.e.polk@jpl.nasa.gov
§Full professor, Departamento de Física Teórica de la Materia Condensada and Condensed Matter Physics Center (IFIMAC), r.c.monreal@uam.es
¶Fletcher Jones Professor of Aeronautics and Applied and Computational Mathematics, Graduate Aerospace Laboratories, dim@caltech.edu

experimentally measured temperatures and therefore, this approach constitutes the first successful attempt to simulate a LaB_6 hollow cathode with 2D axisymmetric models for the plasma and heat transfer to the cathode that are self-consistently coupled. This mechanism could govern the neutralization in other cathode technologies where low work function emitters are employed.

Nomenclature

J_D	Net discharge current
V_D	Discharge voltage
j_{ther}	Thermionic emission density
T	Temperature
ε	Total hemispherical emissivity
$\dot{m}_{Xe}$	Xenon mass flow rate
ϕ	Work function
$\phi_{Schottky}$	Modification of the work function due to the Schottky effect
$\bar{z}$	Dimensional coordinate along centerline of the cathode
$T_{insert}(z)$	Temperature distribution along the hollow cathode insert
V_K	Keeper voltage
e	Electron charge
k_B	Boltzmann constant
D	Richardson-Dushman law constant

I. Introduction

Reaching further, going faster and delivering heavier payloads are the ultimate goals of the design of any space vehicle. In order to improve the current technical capabilities and enable more ambitious deep space missions, NASA is investing in high power electric propulsion systems. Scalable arrays of Hall thrusters are at the heart of these propulsion systems.

Hollow cathodes are among the basic components necessary for Hall thruster operation, and therefore cathode lifetime is a major determinant of thruster lifetime. There are several cathode failure processes which are still not fully understood and a better understanding of the different physical mechanisms that govern cathode discharges is necessary. Thermionic emission of electrons is the most fundamental mechanism regulating cathode discharges. Thermionic emission is tightly dependent on the work function of the emitting surface of the cathode. Cathodes composed of a porous tungsten emitter impregnated with barium-calcium-aluminate mixture have been used extensively in space applications. This technology maintains a relatively low work function during the operation of the cathode, conferring a long lifetime. LaB_6 cathodes are a promising alternative with several advantages over tungsten cathodes, which include emitting surface oxides self-cleaning, greater resilience to contamination, and low work function. A low work function is essential for electron emitters because it enables operation at a lower temperature for a given emission current, which reduces the evaporation of the emitting material and thus increases their useful lifetime.

Hollow cathodes are thermionic emitters classically modelled with the Dushman-Richardson law (Eq. 1[1]). This law relates temperature, emission current density of electrons and work function. Several phenomena must be taken into account when studying the emission characteristic of a hollow cathode, namely 1) the return current of electrons and ions to the emitting surface, 2) the Schottky effect, 3) space charge limitations, 4) temperature variation along the emitting surfaces and 5) work function variation due to evolution of the chemistry and/or crystallographic structure of the emitting surfaces.

$$j_{ther}(\phi, T) = DT^2 \exp\left(\frac{-e(\phi - \phi_{Schottky})}{k_B T}\right), \tag{1}$$

where T is the temperature at the emitting surface, $D = 29A/cm^2K^2$ to account for the work function temperature dependence, k_B is the Boltzmann constant, ϕ is the work function of the material, $\phi_{Schottky}$ is the reduction in the work function due to the external electric field and e is the electron charge.

In order to illustrate the thermionic behavior of a cathode, a simple analysis can be done with the following assumptions:

1. No net return current (contribution from plasma electrons and ions)
2. $\phi_{Schottky} = 0$
3. Current is not space charge limited
4. Uniform temperature along the emitter
5. Uniform work function along the emitter

Fig. 1 shows a study of thermionic emission current density with temperature and ϕ as a parameter for a range of temperatures between 1200 and 1600 $^{\circ}C$ for LaB_6. The emission current density for a 2.54cm long insert with inner diameter 6.35mm and net discharge current of 25A is shown, as well as the range if a net return current of +/-10 and 15% are considered. The temperature of the insert for this configuration when a $\dot{m}_{Xe} = 13 sccm$ has been measured experimentally[2] and the range is shown as well.

This simplified example shows that the return current and temperature distribution are of great importance. In fact, all of the aforementioned physical details must be considered to develop a more accurate description of LaB_6 hollow cathode operation. We can observe though that the work function for LaB_6 hollow cathodes operated with an internal gas discharge must be lower than the previously reported value of 2.66 eV[3] for polycrystalline LaB_6 operating in vacuum. Our previous estimate of the work function for this operating point was ~2.19eV, where assumptions 1,2,3 and 5 were used and the temperature profile along the insert ($T_{insert}(z)$) was extrapolated from three thermocouple measurements using a second degree polynomial fit.

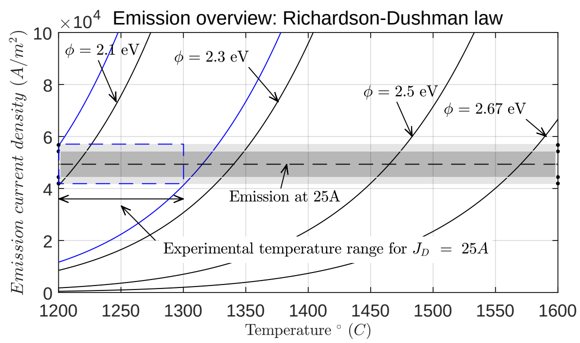

Figure 1: Thermionic emission sensitivity analysis for Richardson-Dushman law. Uniform emission at $J_D = 25A$ is shown with a +/-10% net return current (dark shaded area) and a +/-15% net return current (lighter shaded area). Experimentally measured temperature range of the insert at $J_D = 25A$ is also shown, as well as the range of work function possible for it.

In order to improve the determination of the work function in a LaB_6 hollow cathode that has reached steady state, it is of a paramount importance to accurately determine the net return current (considering space charge limitations), $T_{insert}(z)$, and the impact of the Schottky effect in the work function. If all of those variables were perfectly known, the work function could be determined with higher accuracy than in our previous work. In the present work we have employed the JPL in-house plasma solver OrCa2D to find the plasma structure inside the cathode, which provides a quantification of the net return current and Schottky effect.

The question of how to accurately determine the temperature distribution is still challenging to answer. Two experimental approaches have helped establishing the aforementioned temperature in our previous work, i.e. type C thermocouples and sapphire fiber optic-based ratio pyrometry. Even though we continue to improve those techniques with more accurate calibrations, the temperature distribution along the emitting surfaces has uncertainties that impact the proper determination of thermionic emission in a significant manner. With regards to the thermocouple approach, it is only feasible to measure the temperature at a few locations along the emitting length of the insert, and then the temperature can be interpolated between those points. However, it is difficult to make thermocouple measurements of the temperature at the ends of the insert, which impacts the estimation of the actual shape of $T_{insert}(z)$. Furthermore, type C thermocouples have a 1% inherent tolerance, which gets worse when they are chained with extension wires, connectors and feedthroughs. The fiber-optic approach also poses challenges in determining $T_{insert}(z)$. Fiber-optics depend on their calibration and a view factor correction method to produce the most accurate temperature profile. When they are used with LaB_6 cathodes, fiber-optics might get coated with La, which could impair their optical properties and shift their calibration. In addition, accurate view factor correction of the unfiltered signal relies on knowledge of the temperature distribution of all the surfaces within view of the insert, data which are not available.

We have developed a third method to improve our understanding of the temperature distribution along the insert and the fidelity of the plasma structure inside hollow cathodes in general, producing a more self-consistent simulation package for hollow cathodes with internal gas discharge. A high fidelity thermal model of the cathode built using the COMSOL Multiphysics® heat transfer module was experimentally validated and coupled with the in-house OrCa2D plasma solver. An iterative coupling of the two codes is possible due to the slower time scale of the thermal response of the cathode compared to the much faster plasma behavior. Using this coupled OrCa2D-COMSOL solver, we can simulate the temperature distribution that is self-consistently produced at steady state during cathode operation for any geometry, materials used and operating conditions that we establish. Combining the OrCa2D-COMSOL coupled solver with the aforementioned experimental methods brings a significant improvement to the cathode temperature determination problem.

In our previous work[4] we showed how this self-consistent approach could not replicate the experimental temperature measurements of the cathode insert run at the appropriate operative points. The sensitivity analysis done on that work proved that the root of the discrepancy was neither lack of fidelity in the thermal model, nor due to sensitivity of the parameters used as boundary conditions for the plasma solution. However, the sensitivity of the solution to work function variations along the emitter and the effect of the energy accommodation factor were not studied. Additionally, resonant neutralization and 0% survival probability for the ions that form the return current to the cathode was assumed. In the present work we studied the sensitivity of the self-consistent model to variation in the work function along the insert, the effect of the energy accommodation factor, as well as a two step neutralization mechanism. The results show several possible scenarios to find agreement with the experiments.

II. Methods

The overall strategy used to couple both codes can be seen in Fig. 2. MATLAB® 2018a was used as the main framework from which OrCa2D and COMSOL simulation packages are controlled and where the overall decision making takes place. The general process of finding a plasma solution which is consistent with the thermal characteristics of the hollow cathode requires several global simulation/iteration steps.

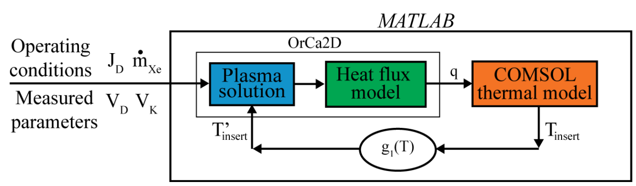

Figure 2: Overview of the strategy used to compute the coupled solution that includes plasma and thermal models

A global iteration step starts when OrCa2D is provided with a temperature distribution for the insert and the plasma solution is then obtained for the particular operating point. At that point, OrCa2D produces the heat fluxes to the walls of the cathode from electrons and ions. Those fluxes are then input into the COMSOL heat transfer simulation package where the updated temperature of the insert can be obtained. Then, MATLAB® compares the temperature provided to OrCa2D at the beginning of the global iteration step with the temperature profile that COMSOL has generated using the plasma heat fluxes. If they are not the same, the code creates a new temperature profile using the merging function g_1[4] to input into OrCa2D, which is closer to the one that COMSOL computed in the previous global iteration step. In order to input $T'_{insert}(z)$ into OrCa2D, a fourth order polynomial fit is used. Then, a new global iteration can be computed. The code finishes when the temperature input into OrCa2D and the one computed by the COMSOL heat transfer module differ by a small tolerance. The root mean square error (RMSE) of both profiles is computed and convergence is defined when this value is less than 10. At that point, we conclude that the plasma solution is self-consistent with the thermal model of the cathode.

With this self-consistent solution we are able to capture the details of the shape of $T_{insert}(z)$, along with a high fidelity estimate of the net return current and Schottky effect. The details of the chemical evolution of the surface is capture by the input of a work function profile along the emitter surface and the definition of the heat fluxes that the plasma produces and input in the thermal model.

A. Hollow cathode thermal model

The thermal model used in this study was created using COMSOL Multiphysics® V5.3a. The geometry was built using SOLIDWORKS® 3D CAD 2016 and imported into COMSOL. Two "Physics" modules were used to model heat transfer by conduction and radiation between components, "Heat Transfer with Surface-to-Surface Radiation" and "Heat Transfer in Thin Shells". The meshing approach was based on a parameterization using a combination of maximum sized elements in the edges of the domains and "extremely fine refinement" for the interior of the domain. The thermal model was written in batch mode in Java, enabling MATLAB® to dynamically create and execute thermal models with any configuration. An example of the solution of such a strategy is shown in Fig. 3.

1. Geometry

The geometry of the cathode thermal model is a 2D axisymmetric approximation of the actual cathode geometry. The different parts are shown in Fig. 4, where part number 1 is the insert, 2 is the cathode tube, 3 is the orifice plate, 4 is the heater, 5 if the radiation shielding and 6 is the keeper. The mounting plate (Part 7) is a fictitious boundary at which a fixed temperature equal to that measured at a corresponding point on the cathode tube is specified. In reality the cathode is attached to an aluminum block 0.5" further upstream.

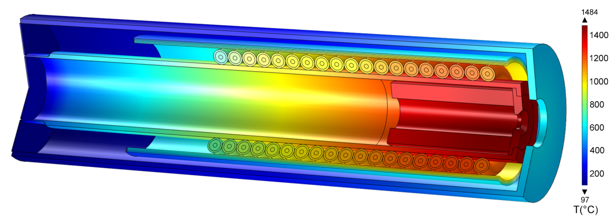

Figure 3: Temperature distribution created with COMSOL (example).

The heater coil is manufactured with an inner diameter slightly smaller than the cathode tube outer diameter so it presses against the tube when installed around it. Because the heater and cathode tube are both made of pure Ta and are pressed together, during operation at high temperature they eventually fuse to each other. This interaction between the two parts was modelled with a point contact between the individual heater coils and the cathode tube. Thermal conductivity and total hemispherical emissivity values for the different materials used in the cathode construction were obtained from the literature. For more information about the thermal model, please consult.[4]

2. Thermal fluxes - the interface with the plasma solver

Heat from the plasma is input into the model as heat fluxes along the surfaces shared by both codes. The approach followed for this interaction is based on extracting the heat fluxes from the plasma at every grid point of the plasma boundary and interpolating their value at every grid point of the thermal model boundary. The total heat input into any surface was used to check the success of the approach.

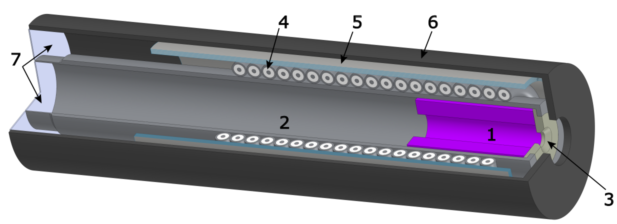

Figure 4: Cathode geometry.

B. Plasma model

All plasma simulations presented herein have been performed with the 2-D axisymmetric solver of the partially ionized gas in hollow cathode discharges called OrCa2D. Development of the code began in 2004 and since then it has been used to simulate numerous hollow cathodes, operating under a wide range of conditions.[5–11] Comparisons with several plasma measurements (e.g.[11, 12]) have helped improve both our understanding of driving processes inside these devices as well as the fidelity of the code.

The physics models, conservation equations and numerical methods in OrCa2D have been described in detail in previous articles[5, 6, 8, 10] and will only be described briefly here. The code solves the conservation laws for three species in the partially-ionized gas: electrons, xenon ions and xenon neutrals. It is assumed that only singly-charged ions are present and that quasi-neutrality prevails except inside sheaths which are handled with appropriate boundary conditions. The Navier-Stokes equations are solved for the neutral gas only inside the cathode up to a transition boundary at which the method to obtain the solution changes to a collision-less approach that assumes neutrals follow straight-line trajectories.[13] The Euler equations for mass and momentum of ions are solved in the entire computational domain. A separate energy equation also is solved for the ions allowing for distinct temperatures between the two heavy species. Ionization, charge exchange and electron-ion collisions are accounted for in the equations and modeled as source or drag terms. The solution for the electrons is obtained from a combination of Ohms law, energy and current conservation equations. An idealized model for the anomalous enhancement in the resistivity, which is now known to occur in the cathode plume[14,15] due the excitement of ion acoustic turbulence (IAT) there, is included in Ohms law. The model is based on the formulations of Sagdeev and Galeev (S&G)[16] and is described in more detail in our companion paper by Mikellides, et al.,.[17]

The emitted electron current density from the insert is specified according to the Richardson-Dushman equation for thermionic emission.[18] The emitter temperature is implemented as a boundary condition in OrCa2D using a 4th-order (or lower) polynomial that provides the temperature as a function of axial position along the emitter. The field-enhanced emission due to the Schottky effect is included as derived in,[6] and its implementation in OrCa2D is described in.[19] The work function must be provided and its value is assumed presently to remain fixed along the entire emitter. It is important to emphasize that net emission is determined not only by the emission current density but also by the current density of electrons and ions that are absorbed by the emitter wall. This is also accounted for in OrCa2D as described in.[5,6] For boundaries that are electrically conducting, electron and ion collection is accounted for in both limits of ion-attracting and an ion-repelling sheaths. This boundary condition was described in detail in.[9] At the anode, current is collected as specified by the discharge current. At the anode, it is also assumed that ions become neutralized after they strike it and return back to the computational region as neutrals with a thermal speed that is based on the specified temperature of the anode.

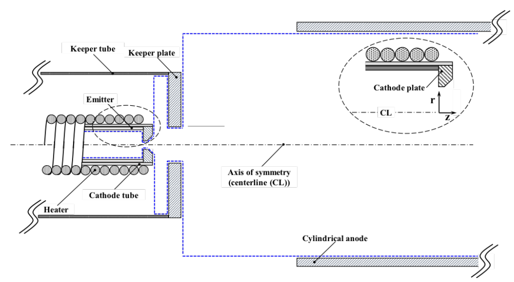

Figure 5: Schematic of the computational domain (blue dashed outline) used in the OrCa2D simulations, in a region near the cathode electrodes and plume (not to-scale).

In the experiments that provided the conditions and measurements for the cathode investigated here, a cylindrical anode was used.[2] The OrCa2D computational domain in the vicinity of the cathode plate and near plume is outlined in Fig. 5. The full domain from a representative simulation of the cathode is shown in Fig. 6. The two figures also provide naming conventions for the various cathode components and boundary conditions that are relevant to this study. The inlet boundary is defined to be at z=0 in the domain. The keeper was set to collect no net current (i.e. it was floating), which was accounted for in the simulations through appropriate boundary conditions. A zero-current condition also was specified at the out-flowing boundaries (Fig. 6). A magnetic field was not applied in the experiments or the simulations.

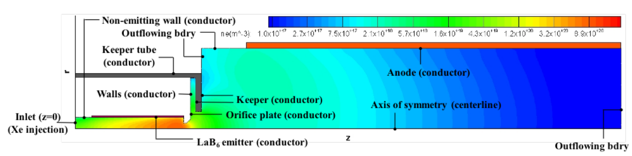

Figure 6: OrCa2D numerical simulation (half) domain showing naming conventions for all relevant boundaries of the LaB6 cathode. (Also shown is the simulation result for the electron number density, n_e (the details of which are described later in this article).

The highest Xe^+ number density expected in the cathode is on the order of $n_{i\_max} = 10^{21}\ m^{-3}$. Using that estimate for the plasma density, the photon mean free path based on the Planck opacity or the Rosseland opacity is much larger than 10 cm and 2.5 m respectively.[20,21] Thus, the plasma is considered transparent and it does not interact with the thermal radiation mechanisms described above.

At every global iteration step, a new temperature profile is input to the plasma solver. OrCa2D was configured to find the plasma solution that provides the keeper voltage that matches the experimentally measured value of V_K. Then, the new heat fluxes associated with the converged plasma solution are input into the thermal model in order to generate an updated temperature profile for the insert ($T_{insert}(z)$). This is one of the many approaches that can be used to update the plasma solution at every iteration. This approach provided the most stable convergence in the global sense because the plasma solution is always close to the one that matches the experimental value of V_K, and only the heat fluxes are being influenced by the small changes in the plasma distribution and the updated value of the work function.

During the simulation, the evolution of the plasma solution is monitored by several numerical probes positioned throughout the computational domain. A convergence criterion has been implemented in OrCa2D that is based on the time-averaged computed variables. The algorithm computes the percent change in the main plasma variables within a specified time increment, from all numerical probes. The simulation is terminated when the maximum percent change is less than a specified value. The MATLAB® framework was built to be able to manipulate this convergence criterion as needed. The current configuration requires the plasma solver to produce more accurate results as the global simulation gets closer to the self-consistent solution. This strategy optimizes global convergence computational time without affecting the fidelity of the final solution.

C. Neutralization model

The inner region plasma consists of three fluids - neutrals, electrons and ions. Depending on the operative point of the cathode, different fluxes of those components reach the internal cathode surfaces exposed to the plasma. These fluxes heat the cathode, thus maintaining operational temperatures. In the cathode used in this study, the main heating thermal load consists of ions returning to the cathode, accelerated in the sheath. The main cooling load comes from the thermionic emission of electrons into the plasma. The emitter and the orifice plate receive approximately the same net heat load. The next relevant heat load is received by the keeper. The electron heating effect is insignificant given the low electron return current collected.

The total amount of energy that ions returning to the cathode bring with them consists of the energy picked up as the ions are accelerated through the potential of the sheath $j_i\phi_{sheath}$, their thermal energy $j_iT_e/2$, and the ionization potential IP of the specific gas used, in our case, xenon. The exact amount of heat transferred to a surface when an ion collides with it depends on the following factors: ion survival rate, energy accommodation factor and neutralization mechanism. Depending on the surface internal electron density profiles where the ions collide, and the energy level of ionized and first excited neutral states of xenon, we anticipate two possible mechanisms to govern the neutralization process of Xe ions upon interaction with the cathode surfaces i.e. one or two step neutralization mechanisms.

Additionally, ion survival probability and energy accommodation factor need to be taken into account. In our case, the low energy of the noble gas ions returning to the surfaces of the cathode (<50eV) indicate that we can assume 0% probability of ion survival rate.[22] However, the energy accommodation coefficient α_{EAC} cannot be neglected. The nature of this coefficient resides on the inelastic behavior of the interaction between ions and surfaces, therefore, it is a function of the incident angle of the ions with respect to the normal of the surface (β). Furthermore, α_{EAC} only affects the potential and thermal energy of the ions, as the energy exchange due to neutralization is independent of the kinetic details of the collision between ions and surfaces. Accounting for this effect, the heat load due to ions interacting with surfaces can be written as Eq. 2. Where α^0_{EAC} is the energy accommodation factor for normal ion incidence and $f(\beta)$ is the function that accounts for deviations with respect to the normal. In this work, we only use the canonical form of $f(\beta) = cos(\beta)$ as the ions become merely perpendicular to the surface due to the strong action of the sheath, and therefore, the results are basically insensitive to the functional form of $f(\beta)$. The energy associated to the neutralization event is accounted for in $N.C.$, which stands for neutralization component.

$$\dot{q}_i = j_{i-return}(\alpha^0_{EAC}\ f(\beta)\ (\phi_{sheath} + T_e/2) + N.C.) \tag{2}$$

1. One step neutralization model

The first mechanism is resonant tunneling neutralization. In this case, incident ions are neutralized as they come closer to the surface by tunneling an electron from the appropriate energy band of the solid into an energy hole of the ion, thus creating a ground state xenon neutral. In this case the energy given to the surface is the ionization potential of xenon minus the work function of the surface $N.C. = IP - WF$, where $IP = E(Xe^+) - E(Xe^0)$

2. Two step neutralization model

The alternative neutralization model consists of resonant neutralization to the first excited state of xenon (Xe^*) followed by Auger de-excitation to the ground state of xenon (Xe)[23] . This mechanism is only possible if the work function of the material is low enough, thus allowing electrons from the appropriate energy level in the material to fill the respective energy hole in the ion, creating an excited neutral. In the case of xenon, the difference between the ionized and the first excited state is $E(Xe^+) - E(Xe^*) = 3.81eV$, according to the NIST database. This means that only the emitter surface can be modelled with this two step neutralization model, as the other surfaces are pure metals and their work function is greater than 3.81eV. The probability of creating excited neutrals is higher than the one to create ground state atoms due to the fact that electrons have to tunnel through a lower potential barrier.

In the first step, the amount of heat exchanged between the ion and the surface is due to the transfer of one electron per ion neutralized, $E(Xe^+) - E(Xe^*) - WF$. During the second step, the excess of energy contained in the excited xenon neutral relaxes to the ground state xenon neutral by transferring that energy to the solid. The electrons in the solid will then be excited with this energy. Depending on the distribution of the energy in the solid, a different population of electrons will be excited and a portion of them will be emitted by means of Auger de-excitation. We model that probability with a parameter, γ_{Auger}. In summary, the total amount of energy deposited in the solid due to neutralization per ion strike is $N.C. = IP - WF - \gamma_{\text{Auger}}(E(Xe^*) - E(Xe^0))$.

As a side effect, electrons are emitted from the solid at a rate $j_e^A = \gamma_{\text{Auger}} j_{i-return}$. These electrons get accelerated away from the emitter by the emitter sheath. This component has to be taken into account when computing the net charge exchange at the emitter surface.

D. Work function distribution

In this work we also studied the dependency of the self-consistent solution on work function distributions along the emitter. This study was motivated by the observation of discoloration along the emitter suggesting chemistry evolution upon to plasma interaction. The impact in the magnitude of the work function or its spatial dependency is difficult to capture experimentally, as we cannot measure the work function or the chemical state of the surface while the cathode is running. However, we decided to study the effect of linear and parabolic work function profiles whose mean magnitude is adjusted according to the self-consistent model needs. The amplitude of those profiles is 0.2eV, as we estimated that this is sufficient to observe the sensitivity of the solution to a plausible real scenario, see Fig. 7.

III. Results and discussion

We employed the novel scheme described above to study the self-consistent solution of a LaB_6 cathode running at J_D=25 A and $\dot{m}_{Xe}$=13 sccm. The keeper and discharge voltage used were the experimentally measured values of $V_K = 4.2V$ and $V_D = 25V$.

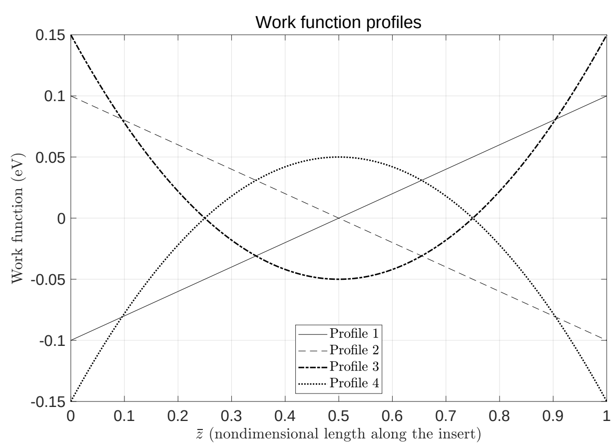

Figure 7: Work function profiles studied in this work.

A. Results

The self-consistent solutions show that the temperature distribution is not greatly affected by the work function profiles utilized in this study. The net effect on the insert temperature for Profile 1 in Fig. 7 is a shifted temperature distribution $\sim 30°C$ colder than the solution with constant work function profile. Similarly for Profile 3, it is $\sim 25°C$ colder. For profiles 2 and 4, the shift is towards hotter temperatures, by $\sim 20°C$ and $10°C$ respectively.

The results also showed that the solution is indeed insensitive to $f(\beta)$ and if $\alpha^0_{EAC} = 0.75$ at every surface of the cathode - the converged solution does not agree with the experimental values as shown in Fig. 9. However, a much better agreement was found when the two step neutralization model was employed. In this case, $\gamma_{\text{Auger}} = 0.85$ was sufficient to find a reasonable agreement with the experimental results, with work function convergence at 2.27 eV. Similar agreement was found when $\gamma_{\text{Auger}} = 0.5$ and $\alpha^0_{EAC} = 0.8$, in which case the work function is 2.25 eV.

Initial plasma solution for the coupled plasma-thermal simulations

To start the coupled plasma-thermal simulations an initial solution of the plasma must be provided. This is obtained with OrCa2D as follows. The mass flow rate and discharge current are required as inputs to the simulation. They are therefore specified directly in the code based on the conditions under which the experiment was conducted, namely 13 sccm and 25 A. To achieve the specified discharge current, an iteration is performed on a single coefficient that determines the level of resistivity enhancement due to the IAT in the cathode plume, as described in more detail in our companion paper by Mikellides, et al.[24] The discharge voltage is set in the simulations at 25 V to match the experiments. The temperature along the emitter $T_{insert}(T)$ is specified using a second degree polynomial fit to measurements obtained by Guerrero, et al.,[2] using three type C thermocouples, see Fig. 9. The simulation iterates on the value of the work function that yields the measured keeper voltage of 4.2 V.

In the simulations presented here, the convergence criterion was set to 0.002%. The steady-state solution for the plasma potential (ϕ), electron temperature (T_e) and neutral number density (n_n) is provided in Fig. 8. The electron number density (n_e) was shown earlier in Fig. 6. The steady state value of the work function was found to be 2.2293 eV, slightly higher than ∼2.19 eV previously estimated.[2] This new value is a more accurate prediction (∼0.04 eV higher) because we have taken into account the net return of electrons and ions to the insert and the Schottky effect. The net return is ∼4.5 A to the insert and ∼0.5 A to the other cathode surfaces, requiring a net thermionic emission of ∼20 A. This means that the net return current is 20.2% of the discharge current for this operating condition. This effect, coupled with the reduction of ϕ due to the Schottky effect, explains the increase in the estimated work function. We can improve this estimate further when we consider the temperature profile that comes from the COMSOL thermal model. We will eventually include the variation of the work function along the insert as well.

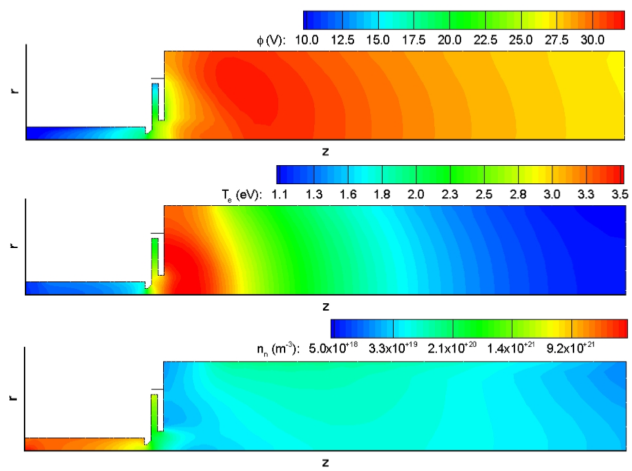

Figure 8: Steady-state solution for the plasma potential (ϕ), electron temperature (T_e) and neutral gas density (n_n) from the OrCa2D simulations with the initial emitter temperature profile shown in Fig. 9 The solution was used to calculate the initial heat fluxes for the coupled plasma-thermal simulations.

As noted earlier, the plasma solution in Fig. 8 is used to calculate the initial heat fluxes for the coupled plasma-thermal simulations. During the coupled simulations the approach to obtain the steady-state OrCa2D solution at each intermediate global iteration remains essentially the same. The exception is that at each iteration a new polynomial fit to the emitter temperature is defined at the OrCa2D emitter boundary, based on the solution provided by the thermal model. With the newly defined temperature, OrCa2D then proceeds to obtain the new steady-state solution by performing the two aforementioned iterations in parallel, namely on the anomalous transport coefficient to attain the specified discharge current (25 A) and on the work function to attain the measured keeper voltage (4.2 V).

B. Discussion

In this work we studied the behaviour of the self-consistent cathode simulation approach with respect to work function axial distribution, ion accommodation coefficient and neutralization mechanisms. We show that in order to find agreement with experimental measurements we need to employ either one of two major assumptions. One assumption is that α^0_{EAC} is smaller than 0.75 if resonant neutralization dominates the charge exchange process of ions that interact with solids for every surface at the cathode-plasma interface. However, we propose that this scenario is unlikely: accommodation coefficients are dominated by the mass ratio between the ions and the atoms of the surface. According to the most extensive data set that we could find in the literature[25] extended to the Xe^+-LaB_6 case, α^0_{EAC} is not expected to be lower than 0.8.

An alternative assumption that leads to an agreement between simulation results and experimental measurements is that the ion-surface interaction is governed by a two step neutralization process described above, with either $\gamma_{\text{Auger}} = 0.85$ and $\alpha^0_{EAC} = 1$ or $\gamma_{\text{Auger}} = 0.5$ and $\alpha^0_{EAC} = 0.8$. In each case, the work function predicted by the simulation platform is 2.27 and 2.25 eV respectively. These values corroborate our previous finding that LaB_6 inserts exposed to plasma in hollow cathodes display enhanced work function[2] with respect to previously reported value of 2.67 eV[3] measured in the diode cell configuration.

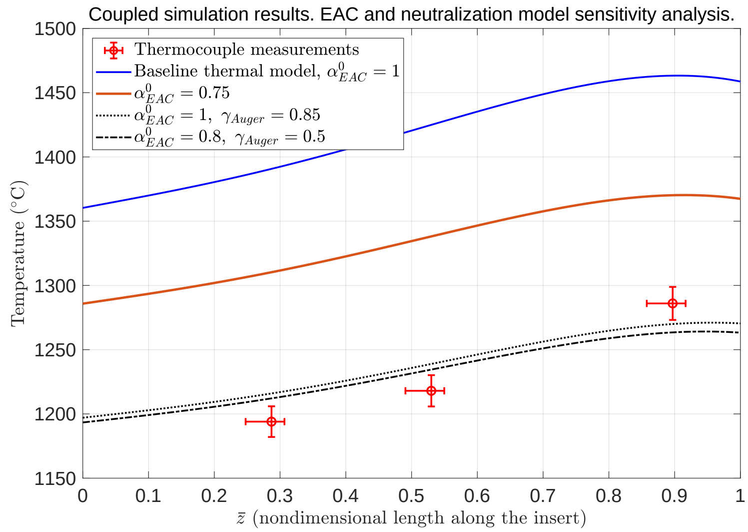

Figure 9: Converged temperature results for the *baseline* thermal model. Sensitivity analysis for EAC and neutralization model. Experimental values shown for comparison.

Two step neutralization is a well-established process in systems comprising low energy ions neutralizing with low work function surfaces. To our knowledge the mechanism of Xe ion neutralization with LaB_6 solids has not been specifically addressed by empirical studies. Experimental work to confirm our model that Xe ions neutralize with LaB_6 solids following a two step neutralization mechanism in similar conditions should be performed. Using simple escape function models to predict the Auger yield in the Xe^+-LaB_6 system, no more than a 30% yield is expected ($\gamma_{\text{Auger}} < 0.3$).[26] This estimation is based on a perfectly flat surface of LaB_6 with net work function of ∼2.25 eV. However, the surface of the insert is not flat, but it is composed of many crystal surfaces oriented at different angles from one another. See figure 10. Therefore, the density of grain boundaries, peaks and valleys is significant. This morphology could explain the additional Auger yield predicted in our simulations. Electric field intensification at peaks will certainly increase the electron yield. The so called atomic-scale lighting rod effect has been shown to be an important source of near field enhancement at atomic scale features, with applications in optical devices and plasmonic nanoestructures.[27,28]

We studied the behavior of the self-consistent cathode simulation approach with respect to work function axial distribution $\phi(z)$. The work function profiles tested did not influence the solution to the extent necessary to find agreement with the experimental results. The work function distribution might be non-uniform in the cathode, but we learned that the self-consistent solution is not heavily influenced by the studied $\phi(z)$ profiles.

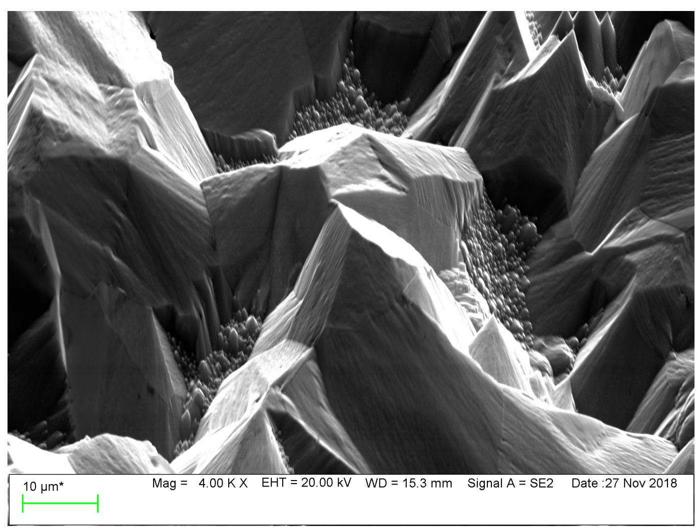

Figure 10: SEM picture of the test sample at the downstream end.

Uncertainties in the plasma model should be identified and their impact in the self-consistent solution should be quantified. This is a very challenging goal given the number of variables involved and the inherently non-linear behavior of the plasma model. It is not clear at this point whether or not such study can be accomplished within a reasonable amount of time given the computational cost of each simulation and the number of variables to be studied.

In conclusion, in order to predict the temperature distribution of the cathode in any configuration and operating condition we still need to identify which of the mechanisms studied here are in fact occurring in the cathode and to what extent they affect the cathode. Experimental work is necessary to obtain that knowledge.

Acknowledgments

We thank Ray Swindlehurst and Nowell Niblett for technical support. Portions of the research described in this paper were carried out at the Jet Propulsion Laboratory, California Institute of Technology, under a contract with the National Aeronautics and Space Administration.

RCM acknowledges financial support from the Spanish Ministry of Science, Innovation and Universities through the Maria de Maeztu Programme for Units of Excellence in R&D (MDM-2014-0377) and the project RTI2018-099737-B-I00

References

[1]Walter H. Kohl, *Handbook of materials and techniques for vacuum devices*, AIP-Press, 1997.

[2]Guerrero, P., Polk, J. E., Richter, M., and Lopez Ortega, A., "Work function reduction in lanthanum hexaboride hollow cathodes operated in gas discharges," *35th International Electric Propulsion Conference*, Atlanta, GA, USA, 2017, pp. 2017–399.

[3]Lafferty, J. M., "Boride Cathodes," *Journal of Applied Physics*, Vol. 22, No. 3, 3 1951, pp. 299–309.

[4]Guerrero, P., Mikellides, I. G., Polk, J. E., and Meiron, D. I., "Hollow cathode thermal modelling and self-consistent plasma solution: work function evaluation for a LaB 6 cathode." *AIAA-SAE-ASEE Joint Propulsion Conference*, 2018.

[5]Mikellides, I. G. and Katz, I., "Wear Mechanisms in Electron Sources for Ion Propulsion , 1 : Neutralizer Hollow Cathode," *Journal of Propulsion and Power*, Vol. 24, No. 4, 2008.

[6]Mikellides, I. G., Katz, I., Goebel, D. M., and Polk, J. E., "Hollow cathode theory and experiment. II . A two-dimensional theoretical model of the emitter region," *JOURNAL OF APPLIED PHYSICS*, 2005, pp. 1–14.

[7]Mikellides, I. G., Katz, I., Goebel, D. M., Polk, J. E., and Jameson, K. K., "Plasma processes inside dispenser hollow cathodes," *Physics of Plasmas*, Vol. 13, No. May, 2006, pp. 063504.

[8]Mikellides, I. G., Katz, I., Goebel, D. M., Jameson, K. K., and Polk, J. E., "Wear Mechanisms in Electron Sources for Ion Propulsion , II: Discharge Hollow Cathode," *Journal of Propulsion and Power*, Vol. 24, No. 4, 2008.

[9]Mikellides, I. G., Goebel, D. M., Snyder, J. S., Katz, I., and Herman, D. A., "The discharge plasma in ion engine neutralizers : Numerical simulations and comparisons with laboratory data," *Journal of Applied Physics*, 2010, pp. 1–12.

[10]Mikellides, I. G., "Effects of viscosity in a partially ionized channel flow with thermionic emission," *Physics of Plasmas*, 2009, pp. 1–10.

[11]Goebel, D. M., Jameson, K. K., Watkins, R. M., Katz, I., and Mikellides, I. G., "Hollow cathode theory and experiment. I . Plasma characterization using fast miniature scanning probes," *Journal of Applied Physics*, Vol. 98, No. 11, 2005, pp. 113302.

[12]Goebel, D. M., Jameson, K. K., Katz, I., and Mikellides, I. G., "Potential fluctuations and energetic ion production in hollow cathode discharges," *Physics of Plasmas*, Vol. 14, No. 10, 2007.

[13]Katz, I. and Mikellides, I. G., "Neutral gas free molecular flow algorithm including ionization and walls for use in plasma simulations," *Journal of Computational Physics*, Vol. 230, No. 4, 2011, pp. 1454–1464.

[14]Mikellides, I. G., Katz, I., Goebel, D. M., and Jameson, K. K., "Evidence of nonclassical plasma transport in hollow cathodes for electric propulsion," *Journal of Applied Physics*, 2007, pp. 1–11.

[15]Jorns, B. A., Mikellides, I. G., and Goebel, D. M., "Ion acoustic turbulence in a 100-A LaB6 hollow cathode," *Physical Review E - Statistical, Nonlinear, and Soft Matter Physics*, Vol. 90, No. 6, 2014, pp. 1–10.

[16]Galeev, R. Z. S. A. A., *Nonlinear plasma theory*, W.A. Benjamin, Inc, New York, 1969.

[17]Mikellides, I. G., Katz, I., Jameson, K. K., and Goebel, D. M., "Numerical Simulations of a Hall Thruster Hollow Cathode Plasma," *30th International Electric Propulsion Conference*, 2007, pp. 1–12.

[18]Dushman, S., "Electron emission from metals," *Phys. Rev.*, Vol. 21, 1923, pp. 623–636.

[19]Mikellides, I. G., Goebel, D. M., Jorns, B. A., Polk, J. E., and Guerrero, P., "Numerical Simulations of the Partially Ionized Gas in a 100-A LaB6 Hollow Cathode," *IEEE Transactions on Plasma Science*, Vol. 43, No. 1, 1 2015, pp. 173–184.

[20]García Rubiano, J., Mendoza, M., Gil, J., Rodriguez, R., Florido, R., Martel, P., and Mínguez, E., "Study of the radiative properties of plasma mixtures of interest for ICF chamber design using the ATMED code," *39th EPS Conference on Plasma Physics 2012, EPS 2012 and the 16th International Congress on Plasma Physics*, Vol. 3, 2012, p. P4.157.

[21]Rodriguez, R., Gil, J. M., Espinosa, G., Florido, R., Rubiano, J. G., Mendoza, M. A., Martel, P., Minguez, E., Symes, D. R., Hohenberger, M., and Smith, R. A., "Determination and analysis of plasma parameters for simulations of radiative blast waves launched in clusters of xenon and krypton," *Plasma Physics and Controlled Fusion*, Vol. 54, No. 4, 2012.

[22]Hagstrum, H. D., "Reflection of Noble Gas Ions at Solid Surfaces," *Physical Review*, Vol. 123, No. 3, 8 1961, pp. 758–765.

[23]Hagstrum, H. D., Petrie, P., and Chaban, E. E., "Interaction of the He+ and Ne+ ions with Ni(100)-K and Cu(100)-K surfaces having variable potassium coverage," *Physical Review B*, Vol. 38, No. 15, 11 1988, pp. 10264–10279.

[24]Mikellides, I. G., Guerrero, P., Ortega, A. L., Goebel, D. M., and Polk, J. E., "Investigations of Spot-to-plume Mode Transition in a Hollow Cathode Discharge Using 2-D Axisymmetric Plasma Simulations," *54th AIAA/SAE/ASEE Joint Propulsion Conference, AIAA Propulsion and Energy Forum: American Institute of Aeronautics and Astronautics*, 2018, pp. 1–23.

[25]Shuvalov, V. A., "Energy accommodation for gas ions on a polycrystalline material," *Journal of Applied Mechanics and Technical Physics*, Vol. 24, No. 6, 1983, pp. 778–785.

[26]Frederick Wooten, *Optical properties of solids*, 1972.

[27]Liao, P. F. and Wokaun, A., "Lightning rod effect in surface enhanced Raman scattering," *The Journal of Chemical Physics*, Vol. 76, No. 1, 1 1982, pp. 751–752.

[28]Urbieta, M., Barbry, M., Zhang, Y., Koval, P., Sánchez-Portal, D., Zabala, N., and Aizpurua, J., "Atomic-Scale Lightning Rod Effect in Plasmonic Picocavities: A Classical View to a Quantum Effect," *ACS Nano*, Vol. 12, No. 1, 1 2018, pp. 585–595.